Global Biogeochemical Cycles

RESEARCH ARTICLE
10.1029/2018GB006029

The Global Marine Selenium Cycle: Insights From Measurements and Modeling

Robert P. Mason[1], **Anne L. Soerensen**[2,3], **Brian P. DiMento**[1], **and Prentiss H. Balcom**[1,3]

[1]Department of Marine Sciences, University of Connecticut, Groton, CT, USA, [2]Department of Environmental Science and Analytical Chemistry, Stockholm University, Stockholm, Sweden, [3]John A. Paulson School of Engineering and Applied Sciences, Harvard University, Cambridge, MA, USA

Key Points:
- Anthropogenic inputs have increased the concentration of selenium in the upper ocean in the last 40 years
- Photochemical degradation of methylated selenium in surface waters decreases the loss of selenium to the atmosphere via gas exchange
- Model results suggest that biological reduction of selenate is occurring in the surface ocean and is an important sink for oxidized selenium

Supporting Information:
- Supporting Information S1

Correspondence to:
R. P. Mason,
robert.mason@uconn.edu

Citation:
Mason, R. P., Soerensen, A. L., DiMento, B. P., & Balcom, P. H. (2018). The global marine selenium cycle: Insights from measurements and modeling. *Global Biogeochemical Cycles*, *32*, 1720–1737. https://doi.org/10.1029/2018GB006029

Received 15 JUL 2018
Accepted 29 OCT 2018
Accepted article online 15 NOV 2018
Published online 3 DEC 2018

Abstract Anthropogenic activities have increased the selenium (Se) concentration in the biosphere, but the overall impact on the ocean has not been examined. While Se is an essential nutrient for microorganisms, there is little information on the impact of biological processes on the concentration and speciation of Se in the ocean. Additionally, other factors controlling the distribution and concentration of Se species are poorly understood. Here we present data gathered in the subtropical Pacific Ocean during a cruise in 2011, and we used these field data and the literature, as well as laboratory photochemical experiments examining the stability and degradation of inorganic Se (both Se (IV) and Se (VI)) and dimethyl selenide, to further constrain the cycling of Se in the upper ocean. We also developed a multibox model for the biosphere to examine the impact of anthropogenic emissions on the concentration and distribution of Se in the ocean. The model concurs with the field data indicating that the Se concentration has increased in the upper ocean waters over the past 30 years. Our observational studies and model results suggest that Se (VI) is taken up by phytoplankton in the surface ocean, in contrast to the results of laboratory culture experiments. In conclusion, while anthropogenic inputs have markedly increased Se in the atmosphere (42%) and net deposition to the ocean (38%) and terrestrial landscape (41%), the impact on Se in the ocean is small (3% increase in the upper ocean). This minimal response reflects its long marine residence time.

Plain Language Summary We measured selenium in water and particles during a cruise in the Pacific Ocean and use this data along with laboratory photochemcial experiments to examine the formation and degradation of the various Se forms in the upper ocean. We also developed a box model to examine how anthropogenic activities have changed the Se concentration throughout the ocean the potential future impacts and to highlight areas of Se biogeochemistry that need further study.

1. Introduction

Human activities have released large quantities of selenium (Se) to the atmosphere through mining and fossil fuel extraction and combustion, but their impacts on the bioavailable Se reservoir in the ocean are not well understood (Chester & Jickells, 2012; Wen & Carignan, 2007). The ocean represents the largest global sink for primary emissions of Se but also acts as a source to other biogeochemical reservoirs through air-sea exchange following the conversion of Se to dissolved gaseous species in both coastal and open ocean waters (Amouroux et al., 2001; Amouroux & Donard, 1996; Mason, 2013; Tessier et al., 2002; Wen & Carignan, 2007).

Atmospheric deposition of Se in both its oxidized forms (Se (IV) and Se (VI)) is the main source to the ocean (Chester & Jickells, 2012; Cutter, 1993; Mosher et al., 1987; Stueken, 2017; Wen & Carignan, 2007). The dominant forms in the ocean are inorganic selenite (Se (IV), predominantly as $HSeO_3^-$) and selenate (Se (VI), as SeO_4^{2-}; Cutter & Cutter, 1995, 2001; Measures & Burton, 1980; Sherrard et al., 2004). The concentration of these forms is lowest (< 0.5 nM) in surface waters and higher at depth. In addition, dissolved organic Se can be a substantial fraction of the total dissolved Se in surface waters, but not at depth (Cutter & Bruland, 1984; Cutter & Cutter, 2001; Sherrard et al., 2004; see Supporting Information (SI), Table S1).

Selenium is an essential element for a wide variety of coastal and oceanic marine phytoplankton, but it can be toxic at high concentrations (Doblin et al., 1999; Harrison et al., 1988; Wake et al., 2012; Wheeler et al., 1982). Selenium-containing proteins and biochemicals are involved in the detoxification of reactive oxygen species and play an important role in the intracellular biochemistry of many trace elements in marine phytoplankton (Khan & Wang, 2009; Zhang & Gladyshev, 2008). Marine phytoplankton preferentially assimilate Se (IV)

relative to Se (VI) via active transport, and they can also assimilate dissolved organic Se (Araie & Shiraiwa, 2009; Baines et al., 2001; Hu et al., 1996). Phytoplankton uptake of Se (VI) is thought to be inhibited in seawater by high sulfate concentrations as Se (VI) uptake involves membrane sulfate transporters (Fournier et al., 2010; Winkel et al., 2015). This pathway is therefore substantially lower than Se (IV) uptake into marine algae (Price et al., 1987; Vriens et al., 2014). Thus, given the similar concentrations of Se (VI) and Se (IV) in ocean surface waters, uptake of Se (VI) should not be significant. However, field data and the similarity of the Se (VI) profiles in the ocean with that of the major nutrients suggest that Se (VI) may be taken up into particles in the surface ocean (Cutter, 2005; Cutter & Bruland, 1984; Measures et al., 1983; Measures & Burton, 1980). We therefore wanted to examine the potential for Se (VI) uptake in the surface ocean in this study. Concentrations of Se (IV) in the surface ocean are low ($<$0.5 nM) suggesting that it could be a limiting nutrient in some regions if Se (VI) uptake is limited (Harrison et al., 1988; Mitrovic et al., 2004; Price et al., 1987; Wake et al., 2012). Once taken up in algae, inorganic Se is reduced to selenide (Se(-II)) and subsequently incorporated into selenoproteins and other organic Se compounds (Gobler et al., 2013; Hatfield et al., 1991; Hatfield & Gladyshev, 2002).

Volatile methylated forms of Se are found in marine surface waters and can evade to the atmosphere (Amouroux & Donard, 1996, 1997; Amouroux et al., 1998, 2001; Tanzer & Heumann, 1991). Degradation of Se-containing biochemicals and proteins leads to their accumulation in the upper ocean. The primary form of methylated Se is dimethyl selenide ($(CH_3)_2Se$). Two additional species (dimethyl diselenide; $(CH_3)_2Se_2$ and dimethyl selenyl sulfide; $(CH_3)_2SeS$) have also been detected (Amouroux et al., 2001; Amouroux & Donard, 1997; Wen & Carignan, 2007). While the formation pathway for methylated Se compounds has been suggested to be analogous to that for dimethyl sulfide ($(CH_3)_2S$ (Carpenter et al., 2012; Stefels et al., 2007), recent results suggest that bacteria, either independently or in association with marine phytoplankton, may be more important for the production of methylated Se compounds (Luxem et al., 2017). In addition, methylated Se has been correlated with both $(CH_3)_2S$ concentrations and coccolithophorid abundance in the North Atlantic, indicating that variability in formation also depends on the phytoplankton community composition (Amouroux et al., 2001), as is found for $(CH_3)_2S$.

The fate of reduced and methylated Se species in the upper ocean is determined by the balance between surface ocean evasion, removal in association with sinking particles, and degradation into inorganic Se species within the water column. Reduced Se, mainly present as volatile and dissolved organic Se(-II) compounds, is concentrated in surface waters and is undetectable at depth (Cutter & Bruland, 1984; Cutter & Cutter, 2001; Table S1). Both Se (IV) and Se (VI) exhibit nutrient-like vertical profiles in the surface ocean (Sherrard et al., 2004, and references therein). If Se (VI) is not readily assimilated by plankton (Araie & Shiraiwa, 2009; Hu et al., 1996), its nutrient-like profile could reflect either export in association with suspended particulate matter as found for nonnutrient elements such as Hg and Pb, or another mixed layer sink. In this study one focus was therefore the sources and sinks for Se (VI) within the ocean.

The main objectives of the current work were to (1) perform field, laboratory, and modeling studies to better characterize the reservoirs and fluxes of Se in the ocean; (2) better characterize the potential for photochemical redox cycling between Se (VI) and Se (IV) in the upper ocean, and the rate of photochemical degradation of volatile methylated Se; and (3) assess the impact of anthropogenic emissions on marine concentrations of Se. To accomplish these, we measured Se in seawater samples from the equatorial Pacific and used field and laboratory photochemical incubation experiments to examine transformations of inorganic and methylated Se compounds in marine waters. We combined these results with existing information to develop a geochemical box model of the global Se cycle and used the model to improve our understanding of factors influencing the speciation and distribution of Se in the upper ocean and the major pathways for interconversion between the different forms of Se. We furthermore examined the importance of historic anthropogenic Se inputs to the ocean on marine Se concentrations and species distributions, and assessed the extent to which anthropogenic sources have impacted the concentration of Se in the ocean.

2. Experimental Methods

2.1. Field Measurements and Analytical Methods

Water samples were collected using a trace metal clean rosette from eight stations occupied in the tropical North and South Pacific during the *Metzyme* cruise from Hawaii to Samoa (1 to 24 October 2011; 20°N to 15°S;

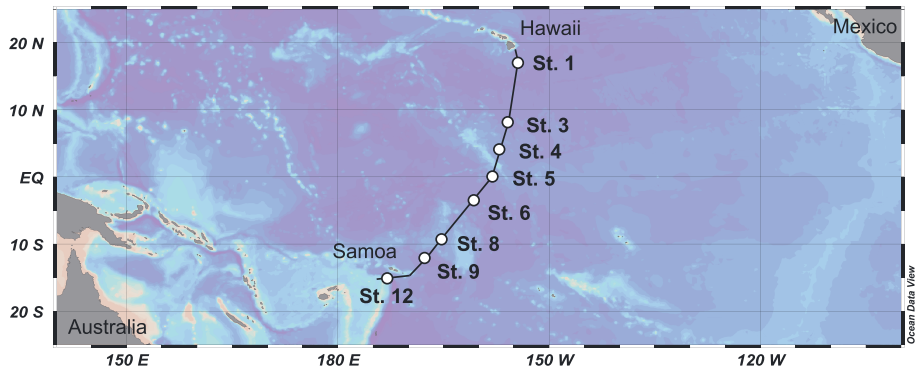

Figure 1. Cruise track showing the locations of the stations during the cruise. Underway surface samples were collected during the entire cruise. Selenium was sampled at Stations 1, 3, 4, 5, 6, 8, 9, and 12.

Figure 1; Munson et al., 2015). Surface water samples were obtained using water collected at 5–10-m depth from the ship's underway sampling system. Particulate samples were collected using McLane in situ pumps from six stations occupied during the cruise at depths up to 900 m, with ~1,000 L filtered per deployment. Water was filtered on board (0.2 μm), acidified to 0.5% HCl (trace metal grade), and transported to the University of Connecticut for analysis. All samples were stored refrigerated (4 °C) and under dark conditions prior to analysis.

Dissolved Se speciation was determined within 6 months of collection following established methods (Cutter & Bruland, 1984; Cutter & Cutter, 2001). The method relies on selective hydride generation of hydrogen selenide using sodium borohydride. Se (IV) is first determined after acidification with 4 M HCl. Total inorganic Se (Se_I) is then determined by boiling samples in 4 M HCl for 15 min to reduce Se (VI) to Se (IV), followed by the same hydride generation step as for Se (IV), and thus, Se (VI) is calculated as the difference between Se_I and Se (IV). We used a PS Analytical Millennium Excalibur instrument equipped with a specific high discharge Se lamp that relies on atomic fluorescence for detection.

Concentrations were calculated based on a calibration curve (R^2 typically $>$0.99). The detection limit, based on 3 times the standard deviation of blank samples, was 0.43 nM for Se (IV) and 0.15 nM for Se_I. The relative standard deviation (RSD) of triplicate sample measurements averaged 11% for Se (IV) and 6% for Se_I following sample reduction. Standard spike recoveries averaged 106% (5% RSD) for Se (IV) and 100% (8% RSD) for Se (VI) standards analyzed as Se_I; Se_I reduction duplicates averaged 7% relative difference.

In most cases in the literature Se speciation analysis has been completed at sea, although there are published data for samples acidified at sea and analyzed up to 6 months later (e.g., Cutter & Cutter, 2001). We, however, found that our results from the inorganic Se speciation analysis were different from those in the literature for the region of study (Cutter & Bruland, 1984; Measures et al., 1983; Measures & Burton, 1980). Specifically, Cutter and Bruland (1984) measured inorganic speciation and organic Se in surface waters close to our cruise path (between Hawaii and Tahiti) in 1980. Organic Se was determined by Cutter and Bruland (1984) as the difference between total dissolved Se (Se_T) and Se_I, and Se_T was quantified after determination of inorganic species by the further boiling of the 4 M HCl solution for 1 hr after the addition of a potassium persulfate solution (Cutter & Bruland, 1984).

Overall, the sum of our measured values (i.e., measured Se (IV) + Se (VI)) was not statistically different (*t* test, $\alpha = 0.05$) from the total filtered concentrations (Se_T) for the previous cruise in 1980: 0.65 ± 0.29 nM in 1980 ($n = 16$) and 0.59 ± 0.22 nM for our data ($n = 32$). Additionally, our Se (VI) data (0.35 ± 0.23 nM) were not statistically different ($\alpha = 0.05$) from the earlier measurements (0.22 ± 0.26 nM; Figure S1). Therefore, while our Se (IV) values were much higher than the 1980 data (≤0.01 nM [their detection limit]), they are comparable to the previous measurements of Se (IV) + Se_{org} (0.43 ± 0.14 in 1980 and 0.28 ± 0.13 nM in 2011). This suggests that the organic Se in our samples was oxidized to Se (IV) during storage resulting in an overestimation of the Se (IV) concentration. While organic Se has previously been detected in samples after a long holding time (Cutter & Cutter, 2001), we believe that this was not the case for our study. Based on the comparison, we conclude that we quantified both inorganic Se (IV) and the organic Se originally

present in the water samples as Se (IV) in our analysis. We therefore report observations only as Se_T in the figures. The data for Se (VI) are presented in the SI in Figure S1 and Table S2.

Particulate Se was measured on subsections of filters collected with in situ pumps (Munson et al., 2015) after microwave digestion (800-W microwave; 20 min at 10% power then 20 min at 20% power to slowly increase temperature). Filters were placed in Teflon bombs with 5 mL of a 10:1 concentrated HNO_3:H_2SO_4 mixture (Zhao et al., 2010). The volume filtered was determined from the total volume filtered by the in situ pump and the fraction of the filter that was analyzed. The detection limit was estimated at 4 pM.

2.2. Photochemical Experiments

Experiments were performed to examine the photochemical transformations of inorganic and organic Se. For the inorganic Se experiments, 5-nM solutions of Se (IV) or Se (VI) were prepared in artificial seawater (Kester et al., 1967) and incubated under light and dark conditions to evaluate the potential for photochemical oxidation and reduction reactions, respectively. Samples in 500-mL quartz flasks were irradiated for up to 1 hr using a 1-kW Oriel solar simulator with an output spectrum similar to equatorial sunlight (see Figure S2a). Samples were stirred using a Teflon-coated magnetic stir bar during the experiments. Temperature (22 ± 3 °C) was controlled using a water bath. Se (IV) and total inorganic Se (and thus by difference, Se (VI)) were analyzed to monitor changes in redox speciation. Results were compared to dark controls (aluminum foil-covered flasks) to evaluate photochemical and dark reactions. All experiments were conducted in duplicate.

Photodecomposition of $(CH_3)_2Se$ was studied in filtered natural seawater under natural and artificial sunlight (Figure S3). It was expected that the other methylated Se compounds would degrade at a similar rate given the likely degradation pathways (Wen & Carignan, 2007), but this was not tested in our studies. Samples were collected from estuarine and shelf sites on the U.S. East Coast and in the Arctic Ocean (for locations see Figure S3). The coastal sites included Berry's Creek in New Jersey, the Penobscot River in Maine, the western Long Island Sound (WLIS), the University of Connecticut's Avery Point campus, Barn Island, and the Connecticut waters of Fishers Island Sound (FIS). In addition, water was collected from offshore sites on the southern New England shelf break (SB) and in the Chukchi Sea of the Arctic Ocean. Collected seawater was filtered (0.2 μm) and stored cold until experiments were completed. Arctic Ocean water samples were collected and stored frozen. Incubations with 3–5 nM of added $(CH_3)_2Se$ were completed under light and dark conditions, as described above. As Se (IV) is the expected stable oxidation product formed from unstable intermediates produced during the degradation reaction (Wen & Carignan, 2007), this product was measured in experimental solutions at the end of an incubation. Before preserving samples for analysis, solutions were flushed with argon to remove any remaining $(CH_3)_2Se$. Samples were then acidified and analyzed for Se (IV) using the method as described above. After longer exposures, the $(CH_3)_2Se$ was essentially completely degraded and the recovered Se (IV) was that expected from the spike addition plus the background Se, indicating that the Se (IV) method of determination recovered all the products of the degradation reaction.

For both inorganic Se and $(CH_3)_2Se$ experiments, studies were repeated with the addition of chemicals known to enhance photochemical reactions. Nitrate (NO_3^-) was added (50–100 μM) to stimulate production of hydroxyl radicals (Zepp et al., 1987) as an oxidant for Se (IV) and $(CH_3)_2Se$. In inorganic Se experiments, Fe (III) (10 nM), dissolved organic matter (DOM; Suwannee River humic acid, [DOC] = 88–166 μM C) and oxalate (0.5 μM) were also added. Fe (III) was added to stimulate the formation of reactive oxygen species (Zepp et al., 1992), while oxalate and DOM were added to examine the potential for charge transfer reactions through the formation of photochemically active complexes. For the inorganic Se studies, NO_3^- and oxalate experiments were repeated with longer incubation times (6 hr) to better evaluate the reaction rates. The wavelength dependence of the $(CH_3)_2Se$ photodegradation reaction was also determined using a UV-blocking film (Figure S2b).

To examine the water column-integrated degradation rate for methylated Se, we applied the results of the HydroLight radiative transfer numerical model (Sequoia Scientific, Inc.) for three representative water bodies: coastal wetlands, estuaries, and the open ocean. Light penetration down to a depth representing 1% of the light intensity at the surface was considered in the model. Rate constants for these water types were represented by values quantified in surface waters from Barn Island, Fishers Island Sound, and Arctic waters, respectively. Surface water total methylated Se concentrations used in the model (Table S3a) are derived

based on limited values in the literature (Amouroux & Donard, 1996, 1997; Amouroux et al., 1998, 2001; Pécheyran et al., 1998; Tessier et al., 2002). The model calculates solar penetration/light attenuation as a function of depth based on water quality parameters, such a chlorophyll *a*, total suspended solids, and chromophoric dissolved organic matter concentrations (Table S3), which influence the extent of light scattering and adsorption in the water column. The modeled wetland waters have higher concentrations of these parameters compared to the estuary, while for the open ocean chlorophyll *a* is the main parameter in the model. The parameterization was initially derived to examine CH_3Hg degradation (DiMento & Mason, 2017) and was transformed to be applicable to methylated Se based on experimental data (see section 3.4) and the relative importance of the radiation spectrum—ultraviolet (UVA, UVB) or PAR (photosynthetically active radiation)—in driving the photochemical degradation of $(CH_3)_2Se$ (Table S3b). Further details on the photochemical experiments and light penetration modeling are given in the SI.

2.3. Model Overview

We developed a six-box geochemical model for the global cycling of Se using data collected as part of this study and a literature synthesis of reservoirs and fluxes (Figure S4). The model framework was adapted from Amos et al. (2013, 2015), who used it to examine the global cycling of Hg. It includes reservoirs representing the atmosphere, terrestrial environments, the coastal ocean, the surface ocean mixed layer (~50 m), the subsurface ocean (50–1,000 m), and the deep ocean (1,000 m to the bottom).

The model includes four main forms of Se: (1) dissolved selenate, Se (VI); (2) dissolved selenite, Se (IV); (3) dissolved reduced Se, SeR, which consists of volatile methylated Se compounds, hydrogen selenide (H_2Se), elemental Se (Se(0)), and other organic Se compounds; and (4) particulate-associated Se, SeP. We estimated external inputs, reservoirs, and exchanges/losses of different Se species for each model compartment based on data from this study and a review of previously measured concentrations and fluxes (Table S4). We used the mass budgets to derive first-order rate coefficients and create a set of coupled first-order differential equations to simulate temporal changes in chemical species following Sunderland et al. (2010). Processes in the model include (1) natural and anthropogenic emissions, (2) chemical transformations between different forms of Se in all compartments, and (3) transport of Se between the reservoirs, including advective transport between ocean reservoirs through seawater circulation and settling of suspended particulate matter. The specifics are detailed below and in the SI text section 2.

2.3.1. Atmosphere

Atmospheric Se species represented in the model (Table S4) include Se (IV), Se (VI), and reduced Se species (Figure S4). Both Se (IV) and Se (VI) are predominately associated with aerosols in the atmosphere but are mostly dissolved in wet deposition (Arimoto et al., 1997; Scudlark & Church et al., 1997; Wen & Carignan, 2007). Deposition mainly consists of inorganic Se species (Cutter & Church, 1986) and is dominated by wet deposition over the ocean (Cutter, 1993). We did not explicitly include particulate Se species in the atmospheric compartment of the model for simplicity. Terrestrial and oceanic Se emissions to the atmosphere occur as methylated Se species (SeR, e.g., $(CH_3)_2Se$), which have a short atmospheric residence time (hours) and degrade into inorganic Se species (Wen & Carignan, 2007; Winkel et al., 2015). Anthropogenic and geogenic emissions are predominantly reduced inorganic Se species (Se(0) and H_2Se), which are rapidly oxidized (lifetime $<$1 day) to Se (IV; Wen & Carignan, 2007, and references therein).

2.3.2. Ocean

Modeled Se forms in the ocean include SeR, SeP, Se (IV), and Se (VI; Table S4 and Figure S4), based on the literature (Table S1). The primary pathway for methylated Se species formation in the surface ocean is through the uptake of inorganic Se by phytoplankton and conversion into organic compounds (Se-containing amino acids and proteins), which are further degraded into the methylated compounds (Amouroux et al., 2000). The particulate fraction (SeP) in the model includes both inorganic and organic Se incorporated into phytoplankton, other organisms and detritus due to direct uptake or partitioning of dissolved species to solids, while in the model SeR refers to the dissolved reduced fraction (methylated Se and other reduced compounds released from organisms). There is limited information in the literature on the relative fraction of organic Se in the ocean (Table S1), and the method of determination, which relies on decomposition of this fraction to inorganic Se using strong oxidants (Cutter & Cutter, 1995; Sherrard et al., 2004), does not provide information about the specific compounds that make up this fraction. It is assumed to be primarily degraded biochemicals from Se-containing proteins and other biomolecules

(Stueken, 2017). Clearly, while this fraction is modeled as one pool, the lack of detailed understanding about the chemistry of this pool is a limitation of the study and more research is needed to gain a better understanding of the pathways of degradation of organic Se compounds produced by microorganisms in the ocean. Formation pathways for volatile methylated Se compounds are from the direct degradation of Se-containing proteins and biomolecules (Luxem et al., 2017). The inclusion of a Se (VI) phytoplankton uptake pathway in the surface ocean of the model is based on observational constraints of measured speciated Se concentrations in seawater, even though many studies suggest that Se (VI) is not assimilated into marine phytoplankton (e.g., Araie & Shiraiwa, 2009; Danbara & Shiraiwa, 1999; Hu et al., 1996; see section 3 and Table S1), especially in the presence of sulfate (Fournier et al., 2010), which is consistent with field data (Cutter, 1992, 2005; Measures et al., 1983). This is discussed further below (section 3.2).

Air-sea exchange is an important component of the cycling of Se in the surface ocean. This flux was estimated based on measured concentrations of methylated Se species (a fraction of the SeR reservoir) in the surface ocean, the results of the photochemcial degradation studies and gas exchange calculations using the Wilke-Chang approximation for the diffusion coefficient and the gas exchange parameterization of Nightingale (Amouroux et al., 2001; Amouroux & Donard, 1996; Nightingale & Liss, 2004; Soerensen et al., 2010), along with previous estimates (Wen & Carignan, 2007). Estimates of deposition of Se (IV) and Se (VI) to the ocean are detailed in Table S4. We do not include SeR in model compartments representing the deep ocean and coastal zone since these species are not above detection limits in these environments (Cutter & Bruland, 1984; Cutter & Cutter, 1995; Conde & Alaejos, 1997; Table S1). Advective and diffusive fluxes between compartments are based on water mass circulation and concentration gradients, respectively, which were derived based on Amos et al. (2015) and detailed in the SI. Vertical SeP fluxes in association with settling solids are derived from measured Se/C ratios (e.g., Cutter & Bruland, 1984) and our measurements. Riverine inputs to the coastal zone and the fraction exported to the surface ocean were based on estimates from prior work (Table S1; Chester & Jickells, 2012; Gaillardet et al., 2003).

2.3.3. Terrestrial Ecosystems

Terrestrial Se species in the model include Se (IV), Se (VI), and SeR (Table S4 and Figure S4). The SeR fraction supports the primary atmospheric flux from terrestrial systems (Winkel et al., 2015, and references therein), and deposition to terrestrial systems occurs as Se (IV) and Se (VI) (Table S4). To simplify the modeling, SeR here accounts for both the particulate Se fraction and other organic Se compounds and there is no separate SeP pool.

2.3.4. Natural and Anthropogenic Emissions

Natural and anthropogenic Se emissions are used to force the box model to simulate preindustrial to present-day changes in the global Se budget. Natural emissions are assumed to be constant over time and are based on estimates from Floor and Roman-Ross (2012) that used the Se/S ratio in geogenic emissions to constrain releases.

Anthropogenic emissions are based on a present-day (2008) ratio for anthropogenic:natural Se emissions of 0.45 detailed in Wen and Carignan (2007). From 1850 to 1980 we scale total emissions by the trajectory of global coal combustion as shown in Figure S5. Between 1980 and the present we account for declining releases due to the implementation of control technologies on coal-fired utilities by decreasing the emissions by 0.01 Gmol/decade from the maximum of 0.22 Gmol/a. This trend mimics the global decrease in SO_2 emissions from coal combustion, as the dominant form of Se in anthropogenic emissions is gaseous Se (Wen & Carignan, 2007). In the atmosphere, geaseous Se is rapidly oxidized and becomes bound to aerosols soon after emission (Wen & Carignan, 2007). Its depostion is therefore controlled by dry deposition of particles and scavenging by precipitation, as discussed above.

3. Results and Discussion

3.1. Pacific Ocean Field Observations

Figure 2 shows total dissolved Se (Se_T) in surface water (Figure 2a) along the Pacific cruise track (Figure 1) and with depth for the stations sampled (Figure 2b), as well as particulate Se profiles (Figure 2c). In Table S2, surface water Se_T and Se (VI) concentrations are broken down into regional averages, as partitioned by Soerensen et al. (2014) based on the salinity, temperature, density, and fluorescence profiles (Figure S6). They are compared to the values obtained by Cutter and Bruland (1984) in Table S2. Surface Se_T

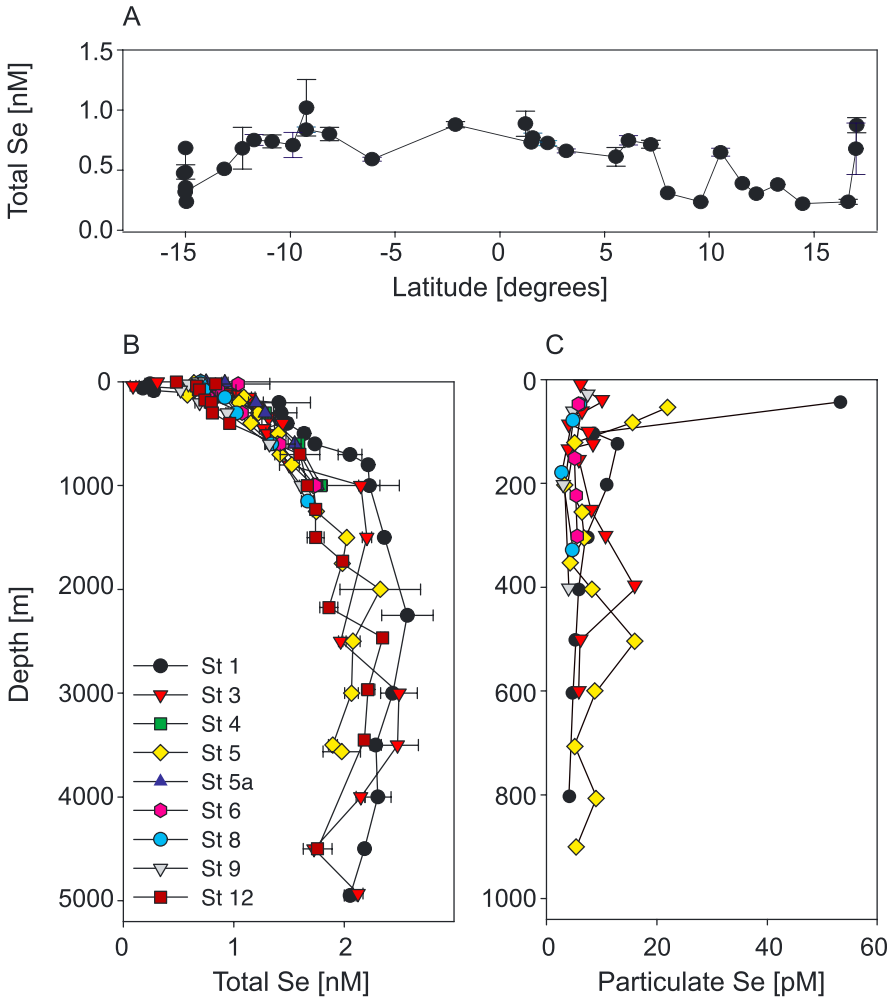

Figure 2. (a) Total dissolved selenium (Se) concentrations in surface waters from the underway sampling system. The variability around 15°S is caused by the cruise track being east to west in the latter part of the cruise (Figure 1). (b) Vertical profiles for total dissolved selenium at all the stations occupied during the 2011 Metzyme cruise (average and standard deviation for replicate analysis). (c) Particulate selenium concentrations measured in the upper ocean during the Metzyme cruise.

concentrations ranged from 0.48 to 0.77 nM (Figure 2a). We suggest that elevated concentrations at the equator are a result of equatorial upwelling, as deeper water is enriched in Se, as suggested by Cutter and Bruland (1984). Atmospheric inputs of Se are an important source to the ocean, and Se (IV) is the dominant species in wet deposition (Cutter, 1993; Cutter & Church, 1986; Wen & Carignan, 2007). The highest precipitation along the cruise track was found in the Intertropical Convergence Zone (ITCZ; low-density and salinity region; Figure S6), and Soerensen et al. (2014) found that mercury was elevated in this region due to wet deposition inputs. However, we do not observe an increase in Se_T in this region. We propose that high productivity at the ITCZ, as indicated by fluorescence measurements (Figure S6), leads to a faster removal of Se (IV) there than in the surrounding regions. This sink, together with the high input from subsurface water in the equatorial region, could mask a clear signal from elevated atmospheric deposition to the ITCZ.

Figure 2b shows that Se_T has a characteristic *nutrient-like* profile with depletion at the surface and increasing concentrations with depth, as found in many previous studies (Sherrard et al., 2004; Cutter & Cutter, 1995, 2001; Measures et al., 1983; Table S1). Surface water concentrations averaged 0.59 ± 0.22 nM (n = 33) and deep ocean concentrations (>3,000 m) 2.1 ± 0.20 nM (n = 11). The Se_T showed little variability across the profiles especially in the upper 1,000 m (RSD 30% for samples between 100 and 1,000 m; n = 60).

Particulate Se concentrations were low (mostly <10 pM; <1% of total Se), with a few high levels near the surface and at 400–500 m (Figure 2c). The profiles do not show a strong change in concentration with depth or latitude, which contrasts with that of carbon (Broecker & Peng, 1982). Using estimates of particulate carbon for the cruise (Gosnell & Mason, 2015; Soerensen et al., 2014), the molar ratio of Se/C for the mixed layer was estimated at $1.3 \pm 1.0 \times 10^{-6}$, comparable with that of other studies and data on phytoplankton Se/C ratios (Cutter & Bruland, 1984; Sherrard et al., 2004, and references therein). Given the order of magnitude decrease in carbon flux between 60 and 500 m, based on sediment trap data from the cruise (Munson et al., 2015), and lower particulate matter at depth, the particulate Se/C ratio must increase with depth. Based on data for particulate concentrations in the deep Pacific Ocean (e.g., Lam et al., 2018), the Se/C ratio is as high as 2×10^{-5} for the deep waters covered during the cruise (>500 m). Such values are higher than, but consistent with, the data from Cutter and Bruland (1984) for the eastern equatorial Pacific (Vertex II; Se/C 0.9×10^{-6} at 50 m) who found that the Se/C ratio was 3–6 times higher for deep waters compared to 50 m. We conclude that even though Se has a nutrient-like profile, it is preferentially retained in particulate matter in deeper waters relative to carbon and other major nutrients.

3.2. Upper Ocean Selenium Cycling

Even though atmospheric input is the dominant external source to the ocean, we find that the mixed layer is depleted in Se. This suggests that it is being rapidly removed from the mixed layer. While both inorganic forms of Se can passively adsorb to particles, they have low partition coefficients ($\log K_D \leq 10^3$) and are not highly particle reactive (Gaillardet et al., 2003; Plant et al., 2003). While Se (IV) is actively taken up by phytoplankton (Harrison et al., 1988; Wake et al., 2012) and is therefore removed from the mixed layer with algal biomass/fecal pellets in a similar manner to other nutrients, the removal mechanisms for Se (VI) are less well understood. Laboratory experiments conclude that Se (VI) is ineffectively taken up by marine phytoplankton so that depletion of Se (VI) in the mixed layer may not be associated with particulate settling. However, as noted above, the strong relationship between Se (VI) ocean profiles and those of the major nutrients suggest that it is (Cutter, 1992, 2005; Measures et al., 1983).

One potential removal mechanism is reduction to Se (IV), either biotically or abiotically. Biotic Se (VI) reduction is theoretically more thermodynamically favorable than sulfate reduction (Mason, 2013) and would occur at a higher pE, even though its concentration is low relative to S (VI) in the ocean. However, biotic reduction would only occur in suboxic environments (e.g., via microbial processes inside large aggregations of particles and marine snow). Studies have shown that Se (VI) reduction may occur via microbial pathways involved in nitrate reduction (Oremland et al., 1999), which has been shown to occur within sinking aggregates (Kamp et al., 2016). On the other hand, the potential for photochemical (abiotic) Se (VI) reduction has so far not been studied. In section 3.4, we therefore examined this potential removal mechanism and its possible impact on surface ocean inorganic Se speciation.

The uptake of Se into phytoplankton and its subsequent conversion into reduced organic Se compounds is likely the primary pathway leading to the formation of volatile compounds, such as $(CH_3)_2Se$, which have been shown to be present in ocean surface waters (e.g., Amouroux et al., 2000, 2001). Volatile Se compounds could subsequently be lost through air-sea gas exchange. To examine the relative importance of gas evasion versus in situ degradation for volatile methylated Se compounds, we performed photochemical degradation studies with $(CH_3)_2Se$ (presented in section 3.4).

3.3. Decadal Trends Derived From Field Observations

We compare our Se_T values from the Pacific Ocean with previous measurements in the North Pacific Ocean (Measures et al., 1980) and find that anthropogenic inputs have elevated Se concentrations in the intervening years. Phosphate profiles from our most northern station (St. 1; 17°N, 154.4°W) match closely with the data collected at the Geosecs station (28.5°N, 121.6°W) in 1977 (Measures et al., 1980; Figure S7) suggesting that these two stations represent the same waters below the surface mixed layer even though sampling was separated by 34 years. We do not compare concentrations in the surface mixed layer as the dynamic nature of this layer makes comparisons of the concentration over time difficult given annual variability. We find no substantial temporal difference for Se_T for the North Pacific deep ocean across the last 40 years (for >3,000 m, 2.28 ± 0.07 nM ($n = 5$) in 1977 versus 2.25 ± 0.14 nM ($n = 5$) in 2011; Figure S7). However, for the subsurface intermediate waters (500–3,000 m) we find a significant increase (10–20%; $p < 0.001$) in Se_T concentration

from 1977 to 2011 (2.10 ± 0.31 (n = 22) and 2.28 ± 0.19 (n = 7), respectively; Figure S7). Similar temporal trends have been seen in intermediate waters for time series studies of anthropogenically released metals (Hg and Pb) in both the North Pacific and North Atlantic Oceans (Boyle et al., 2014; Laurier et al., 2004; Mason et al., 2012; Sunderland et al., 2009). Middepth waters correspond to water masses that circulate on timescales relevant to that of recent anthropogenic inputs (i.e., decades; Sonnerup et al., 2008, 2013, 2015) suggesting that higher middepth concentrations reflect an anthropogenic signal.

While we find no significant latitudinal difference between subsurface water concentrations during our cruise (Figure 2b), individual profiles do indicate higher concentrations in the middepth waters (500–2,000 m) of the Northern Hemisphere (Stations 1 and 3; 1.85 ± 0.35, n = 8) compared to the Southern Hemisphere (Stations 6–12; 1.55 ± 0.18, n = 10). The highest middepth concentrations were found at Northern Hemisphere Station 1, which is most impacted by anthropogenic inputs due to the higher proportion of land, the earlier industrial development in North America and Europe, and the recent heightened industrialization in Asia. In support of the importance of Asian anthropogenic inputs, elevated concentrations of Se (>1 nM) were found in surface waters of the western North Pacific during a cruise in 2002, and these values coincided with elevated concentrations of Ag, Hg, and Pb, and with isotopic differences for Pb indicative of anthropogenic inputs (Laurier et al., 2004; Ranville et al., 2010; Zurbick et al., 2017). Lower concentrations of Se, Hg, Pb, and Ag were found in more remote surface waters during the 2002 cruise compared to those measured in the western North Pacific Ocean. As noted above, the previously measured surface water Se concentrations found on a cruise from Hawaii to Tahiti in 1980 were comparable to our surface water measurements in 2011 for this region. Overall, our results indicate that anthropogenic inputs have resulted in elevated Se concentrations in the North Pacific subsurface ocean over the last 40 years.

3.4. Photochemical Transformations of Inorganic and Methylated Selenium

We found no statistically significant changes in Se (VI) or Se (IV) concentrations during the photochemical transformation experiments with inorganic Se compounds in artificial seawater (Se (IV) oxidation or Se (VI) reduction). Since no transformations were observed in the light or dark, we did not complete further experiments with natural waters for the inorganic Se compounds. We calculated a maximum net rate constant of $<2 \times 10^{-6}$ s^{-1} for Se (IV) oxidation and Se (VI) reduction based on the analytical precision of the Se (IV) and Se_I measurements and a 6-hr incubation time. Our results are comparable to earlier predictions of a slow Se (IV) photooxidation rate, assessed using mass balance considerations and measured ocean concentrations (Cutter & Bruland, 1984; Measures et al., 1980). Given these results, we did not include Se (IV) oxidation or Se (VI) reduction as pathways in our box model. The lack of photochemical reduction of Se (VI) suggests that either biological reduction is occurring in the mixed layer by bacteria in aggregates or at the cell surface of phytoplankton or Se (VI) is being taken up by marine phytoplankton, even though laboratory culture studies do not explicitly support this pathway.

We found that degradation of $(CH_3)_2Se$ was rapid in seawater when exposed to the solar simulator (Table 1a) and natural sunlight (Table 1b). An example of the data obtained is shown in Figure S8, depicting the increase in products, assayed as Se (IV), from the degradation of $(CH_3)_2Se$ as a function of cumulative UV exposure. The degradation pathways in aqueous solution have been little studied, but in the atmosphere the reactions of $(CH_3)_2Se$ with ozone, the nitrate radical, or the hydroxyl radical are thought to initially generate an oxygenated intermediate (CH_3SeCH_2O) that is then decomposed to SeO_2 (i.e., Se (IV)) after further reaction with oxygen (Wen & Carignan, 2007).

We find that reaction rate constants determined under simulated sunlight were significantly higher in waters from the western Long Island Sound (WLIS) than the shelf break (SB; 44.3 ± 3.3 day^{-1} versus 36.6 ± 4.6 day^{-1}; p = 0.018; Table 1a). The addition of NO_3^- significantly increased the reaction rate constants in both waters (WLIS, p = 0.044; SB, p = 0.006). However, the rate constants for samples with NO_3^- added were not significantly different from each other (WLIS: 48.7 ± 2.3 day^{-1}; SB: 52.3 ± 7.6 day^{-1}; $p > 0.05$). The higher initial concentration of NO_3^- in the lower salinity coastal WLIS water might have resulted in the higher rate constant, causing the NO_3^- addition to have less impact. Higher DOC and SUVA values at WLIS on the other hand did not seem to have an effect on rate constants as could have been expected.

Photodegradation rate constants of $(CH_3)_2Se$ determined in natural waters and sunlight ranged from 18.1 to 47.0 day^{-1} (Table 1b and Figure S8). *Dark* samples showed no generation of Se (IV). The highest degradation

Table 1
Photochemical Degradation Rate Constants (± Standard Deviations) for Dimethylselenide for (a) Western Long Island Sound (WLIS) and New England Shelf Break (SB) Sites, With and Without Added Nitrate Completed Using the Solar Simulator, and (b) Incubations of Natural Waters From Various Coastal East Coast U.S. Locations, and for Water Collected in the Surface Arctic Ocean

	Trial	Date	Sal. (ppt)	**DOC (μM)**	**NO_3^- (μM)**	SUVA (L · mg · m)	Rate constant (day^{-1})
(a) Simulated Sunlight							
WLIS	-	9/17/2014	27.2	161	1.5	1.8	44.3 ± 3.3
	+ NO_3^-						48.7 ± 2.3
SB	-	9/12/2014	35.6	85	<0.5	0.9	36.6 ± 4.6
	+NO_3^-						52.3 ± 7.6

	Location	**Date**	**Sal. (ppt)**	**DOC (μM)**	**NO_3^- (μM)**	**SUVA (L · mg · m)**	**Rate Constant ($m^2 \cdot E^{-1}$)**	**Rate Constant (day^{-1})**
(b) Natural Sunlight								
	Berry's Creek	5/21/2016	6.8	397	37.8	3.8	0.407 ± 0.016	28.3 ± 1.1
	Barn Island	6/22/2016	31.0	220	< 0.5	4.8	0.397 ± 0.071	27.6 ± 4.9
	Penobscot River	5/29/2016	22.5	231	3.75	4.3	0.276 ± 0.045	19.2 ± 3.1
	Arctic Ocean	6/18/2016	24.1	162	0.99	1.5	0.260 ± 0.053	18.1 ± 3.7
	Avery Point	7/6/2016	30.1	107.7	< 0.5	1.5	0.629 ± 0.167	43.7 ± 11.6
	Fishers Island Sound	6/30/2016	30.3	245	1.56	1.0	0.676 ± 0.118	47.0 ± 8.2

Note. Ancillary data for salinity, dissolved organic carbon (DOC), nitrate (NO_3^-), and specific ultraviolet absorbance (SUVA) are also shown.

rate constants were measured in waters from Fishers Island Sound and Avery Point, while the lowest were in Arctic and Penobscot River waters. Salinity was lowest at Berry's Creek, where DOC concentrations were highest. NO_3^- was highest in the polluted waters of Berry's Creek and the Penobscot River. Due to low freshwater inputs, Barn Island's high-salinity water closely resembled water from Long Island and Block Island Sound, but with added DOC from the salt marsh. SUVA values were lowest in the Arctic, indicating a different source of DOC in coastal versus oceanic waters.

Photodegradation rate constants were significantly lower for the Arctic and Penobscot River waters ($p < 0.05$) than for the other sites, while Avery Point and Fishers Island Sound were significantly higher ($p < 0.07$) than the rest. There were no apparent correlations between rate constants and salinity, DOC, SUVA, or NO_3^- naturally present at the specific sites. Upon the addition of NO_3^- (50 μM) to water collected from Avery Point, a small (8.8%) but insignificant ($p = 0.45$) increase in the rate constant was observed (Table 1b). This change was consistent with the percent increase observed under simulated sunlight in WLIS water (9.9%), but smaller than the increase observed on the shelf break (42.9%). Overall, results presented in Table 1 suggest that reaction with the hydroxyl radical, which is produced during the photochemical degradation of NO_3^-, is a potential pathway for the degradation of $(CH_3)_2Se$. Such a degradation pathway is consistent with the results of studies with $(CH_3)_2S$, as discussed further in the SI (section S2.5). It is also likely that the other methylated Se compounds, $(CH_3)_2Se_2$ and $(CH_3)_2SeS$, would react at a similar rate given the fact that the initial reaction involves loss of a methyl group. In future studies, the relative stability of the various methylated compounds should also be examined and an experimental setup should allow for changing one variable at the time in order to further decipher the effect of salinity, DOC, SUVA, and NO_3^- on the photodegradation rates of methylated Se compounds.

In experiments using water from Fishers Island Sound, with and without UV exposure (Figure S2b), we found that about 10% of the total photodegradation was due to PAR with the remaining 90% due to UV radiation (Table S3b). We used this result to calculate the depth-integrated degradation rates for our three types of water (coastal wetland and coastal and offshore waters) by modeling water column light penetration using the HydroLight program (Table S3; DiMento & Mason, 2017; see SI for further details). Relative degradation rate constants for the different wavelengths of light were based on our data (Table 1) and that of Taalba et al. (2013) for $(CH_3)_2S$, which also agreed with wavelength dependence found by others (Bouillon et al., 2006; Kieber et al., 1996; Toole et al., 2003, 2004, 2006). Taalba et al. (2013) determined that for surface waters UVA played the largest role in the degradation of $(CH_3)_2S$, accounting for 75% of the rate, while UVB and PAR accounted for the remaining 15% and 10%, respectively.

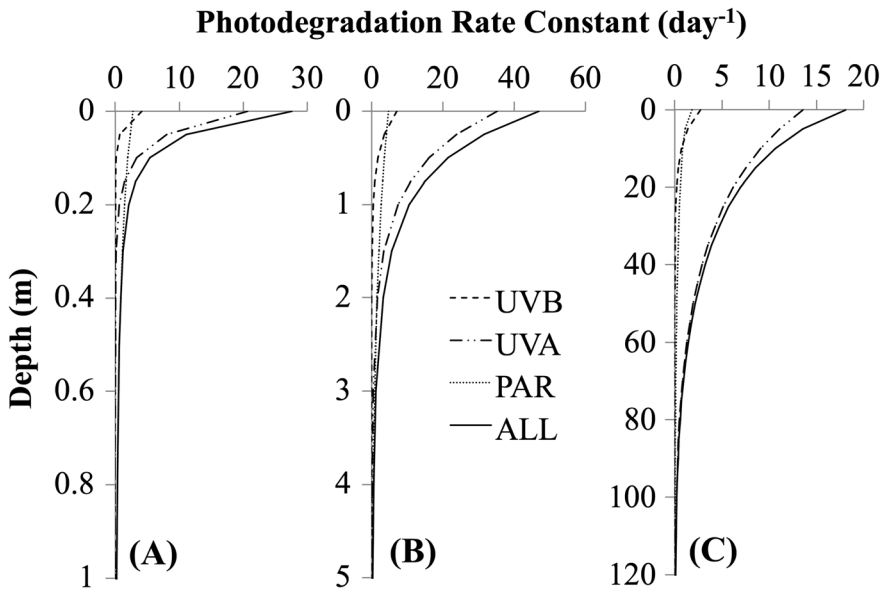

Figure 3. Modeled decrease in dimethyl selenide ($(CH_3)_2Se$) photodegradation rate constants with depth for ultraviolet (UVB and UVA) and visible (photosynthetically active radiation, PAR) wavelengths in coastal (a) wetlands, (b) estuaries, and (c) the open ocean. Rates were calculated based on the modeled attenuation of light, the surface rate constant from corresponding sites in this study (Arctic Ocean, Fishers Island Sound, Barn Island), and the relative importance of each wavelength region from this study and Taalba et al. (2013).

We found that UVA radiation dominates degradation in the surface of all water types (Figure 3), while PAR, less affected by total suspended solid and DOC, plays a more significant role in coastal wetlands and estuarine waters when integrating across the entire photic zone (defined as the depth to 1% of the incident PAR; Table 2). In wetlands, UV radiation accounts for 58% of the $(CH_3)_2Se$ loss, increasing to 91% in the open ocean. The importance of PAR decreases from 42% to 9% over the same transition. Results are consistent with other studies of photochemical degradation in natural systems showing greater importance of PAR in turbid shallow waters than its corresponding degradation rate constant would suggest due to the rapid attenuation of UV radiation (Black et al., 2012; Fernández-Gómez et al., 2013; Poste et al., 2015).

By integrating the degradation rate of $(CH_3)_2Se$ through the photic layer (Table 2 and Figure 3), we estimated a total $(CH_3)_2Se$ loss of 12, 69, and 398 nmol $\cdot$ m^2 $\cdot$ d for wetland, estuarine, and ocean waters, respectively.

Table 2
Light Penetration (to 1% of the Incident Solar Irradiance) and Integrated $(CH_3)_2Se$ Degradation Flux as a Function of Wavelength in Model Coastal Wetland, Estuarine, and Open Ocean Locations

Site	Surface degradation rate (d^{-1})	Wavelength	Light penetration (m)	$(CH_3)_2Se$ loss (nmol m^{-2} day^{-1})	% loss
Wetland		UVB	0.13	0.731	6.16
	27.6	UVA	0.27	6.13	51.7
		PAR	1.92	5.00	42.1
		Total	-	11.86	100
Estuary		UVB	1.63	5.36	7.76
	47.0	UVA	3.14	46.6	67.5
		PAR	8.72	17.1	24.7
		Total	-	69.1	100
Ocean		UVB	33.3	20.8	5.23
	18.1	UVA	107	342	86.0
		PAR	110	35.0	8.79
		Total	-	398	100

Note. Data for the surface degradation rates are taken from Table 3 for Barn Island (wetland), Fisher Island sound (estuary), and the Arctic Ocean (ocean).

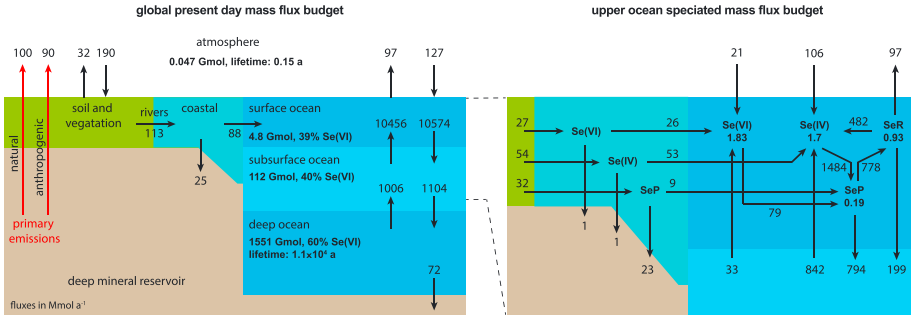

Figure 4. The left figure presents the global 2008 total selenium budget. Natural (geogenic) and 2008 anthropogenic inputs, both from the deep mineral reservoir, reflect the external inputs to the biosphere. The right figure is a blowup of the left figure and shows the speciated budget for the coastal and upper ocean (top 1,000 m). Four selenium species are represented: selenate (Se (VI)), selenite (Se (IV)), reduced organic selenium (SeR), and particulate selenium (SeP). Fluxes are in Mmol/a and reservoirs in Gmol.

This result indicates that photodegradation is a larger sink of $(CH_3)_2Se$ in the open ocean than at coastal sites due to significantly greater light penetration, despite higher $(CH_3)_2Se$ concentrations being modeled for the estuarine and wetland waters. Using the average degradation rate in the photic layer, half-lives with respect to photodegradation were calculated for each of the three model water types. The fastest turnover of $(CH_3)_2Se$ was in the open surface ocean, where the half-life ($t_{½}$) was 0.19 day. In estuarine waters, $t_{½}$ was 0.24 day, and in wetlands it was 0.56 day. The short lifetimes in surface waters suggest that $(CH_3)_2Se$ must be rapidly produced, either biologically or possibly via a separate photochemical pathway (Amouroux et al., 2000, 2001; Guo et al., 2003a, 2003b; Tessier et al., 2002).

The magnitude of $(CH_3)_2Se$ loss due to photodegradation was determined globally by considering the latitudinal variation in solar radiation intensity (Frouin et al., 2012) and ocean surface area (Allen & Gillooly, 2006). Polar seas were corrected for their average ice coverage (DiMento & Mason, 2017). We estimated a global degradation rate of 28.0 Gmol/a, which is used to derive the flux in our box model. More data are needed to further refine this estimate, but the higher degradation to evasion ratio of the methylated Se compounds, relative to that of $(CH_3)_2S$ is consistent with their known reactivity. Variability in $(CH_3)_2Se$ concentrations in the surface ocean along with changes in light penetration due to differences in water quality parameters would impact the predicted $(CH_3)_2Se$ photochemical loss. Changes in $(CH_3)_2Se$ concentrations and degradation rate constants would proportionally change its flux. Changes in chlorophyll concentrations, the primary HydroLight parameter influencing light penetration in the open ocean, would also impact light attenuation and thus $(CH_3)_2Se$ fluxes. For example, a twofold increase or decrease in the chlorophyll concentration results in a 15% decrease or increase in the $(CH_3)_2Se$ flux, respectively. Therefore, our global demethylation rate only serves as an approximation until more data are gathered on the spatial distribution of $(CH_3)_2Se$ in the global oceans. Our degradation flux estimate for the open ocean (~400 nmol $\cdot$ m^2 $\cdot$ d) is large compared to estimates of $(CH_3)_2Se$ evasion from the open ocean (3.2 nmol $\cdot$ m^2 $\cdot$ d for the North Atlantic; Amouroux et al., 2001). Based on these results, we therefore postulate that photodegradation represents the most important sink of volatile methylated Se in the surface ocean.

3.5. Mass Balance Budget Considerations: Selenate Removal From the Mixed Layer

Figure 4 shows the global Se budget for 2008, which was derived using the six-box geochemical model. We arrived at this budget by first simulating natural steady state conditions using preindustrial (geogenic) emissions (100 Mmol/a) and a 5×10^6-year run (Figure S9). From this initial condition we forced the model with historic natural and anthropogenic emissions for the period 1850 to 2008 to arrive at a current day budget (Figure 4 and Table S4). When generating the mass flux budget used to create the box model, we found that in order to balance the surface ocean fluxes and prevent elevated concentrations of Se (VI), it was necessary to include another loss term for Se (VI): a small uptake flux of Se (VI) into phytoplankton (79 Mmol/a; Figure S4). Given the results of the photochemical experiments, we did not include redox chemistry between Se (IV) and Se (VI) within the surface ocean compartment. While there have been reports that phytoplankton do not take up Se (VI) at ambient ocean concentrations (Araie &

Table 3
Average Concentrations for the Ocean Reservoirs Predicted by the 2008 Global Selenium Model

Ocean layer	Se (IV) (nM)	Se (VI) (nM)	Organic Se (nM)	Total diss. Se (nM)
Surface ocean	0.10	0.10	0.05	0.25
Subsurface	0.20	0.13	0.01	0.33
Deep ocean	0.57	0.86	-	1.43

Shiraiwa, 2009; Hu et al., 1996; Fournier et al., 2010; Winkel et al., 2015), the model suggests that there should be a small amount of Se (VI) uptake (~5% of the total uptake as Se (VI) uptake of 1,484 Mmol/a in the model), which is consistent with the relationship between Se (VI) and the major nutrients in most ocean basins (Cutter, 2005; Measures et al., 1983). Such a small uptake of Se (VI) relative to Se (IV) might not be discernable in laboratory culture experiments, but our model results suggest that this is occuring. This conclusion is consistent with that of others based on field measurements (Cutter, 2005; Cutter & Bruland, 1984; Measures et al., 1983).

The alternative explanation for the required sink for Se (VI) would be biotic Se (VI) reduction in the mixed layer, which would have to occur in reduced microzones within aggregates, for example. But Se (VI) reduction has not been observed in the ocean, and our photochemical experiments presented in section 3.4 indicate that it is not likely to be a photochemically driven process. However, Se (VI) reduction has been found in other environments associated with a variety of bacteria (Stolz, 2016; Stolz et al., 2006; Velinsky & Cutter, 1991), but with elemental Se (SeR in the model) being the most likely product (Cutter, 1982, 1992; Oremland et al., 1999). While Se (VI)-reducing bacteria will also reduce nitrate, sulfate reducing bacteria will only reduce Se (VI) if sulfate levels are low, as sulfate uptake and reduction inhibit Se (VI) reduction (Stolz, 2016). Given the higher redox potential for Se (VI) and nitrate reduction, these processes are more favorable within the ocean water column than sulfate reduction. Both nitrate- and iron-reducing bacteria have been found in marine aggregates (Balzano et al., 2009), suggesting that these locations may be important for Se (VI) reduction. Therefore, while we do not include this in the model, we suggest that there may be reduction of Se (VI) inside marine aggregates or other reduced microenvironments or, possibly, reduction at the cell surface, and future studies should investigate these potential pathways.

3.6. Present-Day Selenium Budget

The model results for 2008 are presented in Figure 4. The model was evaluated by comparing the 2008 reservoirs and flows with the best estimates used to build the model (Table S4). We find that the model reproduces the reservoir inventories for each form of Se modeled within a factor of 2 when compared to available information. Table 3 presents the predicted ocean concentrations. The total dissolved Se predictions for the surface ocean (0.25 nM) and the intermediate waters (0.33 nM) are at the low end of what we found in the Pacific Ocean and what is reported in the literature (0.4–0.7 nM for the surface ocean and 0.4–1.2 nM for intermediate waters; Table S1). However, the deep ocean concentration (1.43 nM) reasonably represents the average of values reported in the literature, which range from concentrations of $<$1-nM total dissolved Se for deep waters of the North Atlantic to $>$2 nM for the deep North Pacific Ocean (Table S1). The average ratio of Se (VI)/Se (IV) for the modeled deep ocean (0.65) is also consistent with literature (Sherrard et al., 2004, and references therein; Table S1).

The model predicts a present-day river flux of 113 Mmol/a with particulate Se constituting ~30% of the total flux (Figure 4). The modeled dissolved concentration is ~0.6 nM, and the particulate concentration is 2.5 nmol/g (average log K_D of 3.1), which is consistent with values in the literature (Conde & Alaejos, 1997; Plant et al., 2003; Table S1). The estimated flux is 3.5 times higher than estimated by Gaillardet et al. (2003; 33 Mmol/a) and more comparable with the estimate of Stueken (2017; (80 Mmol/a). However, all the estimates are based on limited information and more studies are needed to further constrain this flux. The model furthermore predicts that 75% (88 Mmol/a) of the Se delivered to the coastal zone via rivers is subsequently transported to the open ocean. This is comparable to the behavior of nutrients and other elements that are mostly in the dissolved phase in river water (Gaillardet et al., 2003; Gordeev & Lisitzin, 2014). The low affinity for the particulate phase means that only 26% (25 Mmol/a) of Se removed to the deep mineral reservoir is removed in the coastal zone (Figure 4), while 74% is removed in the deep ocean

(72 Mmol/a). The major form of Se removed from the coastal zone is particulate Se, primarily associated with organic matter, while in the deep ocean it is from the removal of inorganic Se.

Figure 4 (with the details contained in Table S4) details the relative fluxes for the various fractions of Se in the mixed layer. There is no need to invoke significant Se (VI) reduction or Se (IV) oxidation to balance concentrations if there is uptake of Se (VI) into phytoplankton. Inputs from the atmosphere (127 Mmol/a) are 44% higher than from the coastal zone (88 Mmol/a) and are dominated by inputs of Se (IV; 83%), which is consistent with limited measurements (Cutter & Church, 1986; Wen & Carignan, 2007). The evasion from the ocean surface (97 Mmol/a) is at the lower end of previous estimates (60–400 Mmol/a; Amouroux et al., 2001; Wen & Carignan, 2007), but previous evasion estimates were based on limited data, and we suggest that the global mass balance approach used in the model likely derives a better constrained global estimate.

The major internal fluxes within the ocean mixed layer (Figure 4) are the uptake of Se (IV; 1,484 Mmol/a) and Se (VI; 79 Mmol/a) into plankton, the decomposition of the particulate fraction releasing reactive (organic) Se compounds (778 Mmol/a), and the loss processes for this reactive fraction (evasion and decomposition to Se (IV); 97 and 482 Mmol/a, respectively). The reactive fraction consists of both small molecular weight volatile compounds and larger compounds derived from biochemicals, which will likely degrade less rapidly. Overall, the model predicts that the turnover rate of the reactive pool in the mixed layer is 3 times longer than that of the volatile methylated species. With our new understanding of the importance of the photochemical degradation pathway for the methylated compounds, estimated in section 3.4, and the constraints of the modeled fluxes for the various Se fractions, we calculate that the majority of organic Se is degraded within the photic zone (83%). Not considering photochemical degradation of methylated Se compounds would have caused a large over prediction of the evasion flux of reactive (organic) Se to the atmosphere. We show that photodegradation retains Se in the surface ocean, thereby increasing the overall oceanic lifetime of Se.

Selenium is transported out of the mixed layer via particulate settling (net export of 794 Mmol/a) and surface-subsurface mixing of organic Se (199 Mmol/a). There is a net transport of dissolved inorganic species into the mixed layer due to surface-subsurface mixing and other exchange processes (net flux of 875 Mmol/a). We thus find a net transport of 118 Mmol/a of Se from the mixed layer to the subsurface, illustrating that the subsurface ocean is not in equilibrium with the anthropogenic releases. While anthropogenic releases are quickly distributed to the atmosphere and surface mixed layer (we calculate the lifetime of Se in the atmosphere to be 0.15 a), this is not the case for middepths and the deep ocean (we calculate the lifetime of Se in the ocean to be 1.1×10^4 a). The magnitude of both the exchange and net fluxes between the subsurface and the deep ocean are smaller than those between the mixed layer and subsurface by an order of magnitude and 17%, respectively. We find that the concentrations in the subsurface waters are currently increasing more rapidly than the deep water with regard to their total Se concentrations.

It was not possible to balance concentrations and ratios for the inorganic Se forms in the deep ocean without an additional sink for Se (VI) besides currently established pathways: removal to the sediment (deep mineral reservoir) and mixing into the subsurface waters. We therefore introduced a net reduction of 230 Mmol/a Se (VI) in the deep ocean (Table S4; both Se (IV) oxidation and Se (VI) reduction were included in the model; Figure S4). This corresponds to a reduction rate constant of 2.5×10^{-4} a^{-1}. The most likely pathway is Se (VI) reduction in reduced environments with subsequent burial in association with Se(-II) in inorganic or organic sulfides (Stueken, 2017; Stueken et al., 2015) or Se (VI) reduction in hydrothermal systems with the release of Se (IV) to the overlying water. Also, Se (IV) associates more strongly with oxide mineral phases, and adsorption of Se (IV) to oxide mineral phases in the water column close to sediments, or during early diagenesis, could potentially be an important deep ocean sink for Se (Stueken, 2017). Stueken (2017) estimated burial in the deep ocean to be 90 Mmol/a, somewhat higher but comparable to the model result (72 Mmol/a). Further studies are needed to examine the potential pathways in both the surface and deep ocean in more detail.

3.7. Modeled Historic Changes in Ocean Selenium Concentrations

Figure 5 shows the simulated relative change between preindustrial fluxes and the 2008 budget, with the preindustrial budget shown in Figure S9. We estimate that the fluxes to the atmosphere from primary (both geogenic and anthropogenic) and recycled inputs (ocean and terrestrial inputs) increase the total flux to the atmosphere by 41% (319 Mmol/a compared to 225 Mmol/a in the preindustrial scenario). The atmospheric reservoir inventory is increased by a similar amount (42%), as are the deposition fluxes to both terrestrial

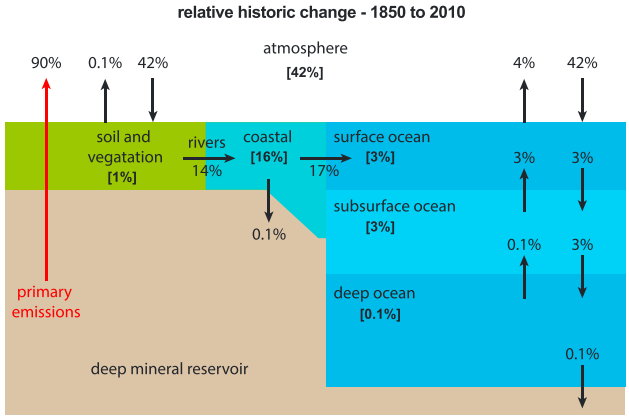

Figure 5. Relative change in concentration and fluxes due to anthropogenic emissions since 1850 as determined by the model. The values in the brackets represent the changes in reservoir amount, while the values with the arrows represent the net change in the fluxes for all species across the boundaries between reservoirs. See Table S4 for details of the fluxes of individual species.

and surface ocean compartments (42%; e.g., from 90 to 127 Mmol/a for ocean deposition; Table S4). However, the relative change in the flux to the atmosphere from the ocean is small (4%) compared to the deep mineral inputs (90% increase). Given the long residence time for the surface terrestrial environment (timescale of 5000 a), the predicted change in the flux, excluding inputs from the deep reservoirs, to the atmosphere of 0.1% is reasonable. For the surface and subsurface ocean, the increase in the reservoir and fluxes is 3%, reflecting that the decadal timescale for mixing of the upper ocean (<1,000 m) is small compared to the duration of the anthropogenic inputs in the simulation (~160 years). Removal from the deep ocean to the deep mineral reservoir is only slightly changed because of the long time needed to transfer the last 160 years of anthropogenic inputs from the atmosphere to the deep ocean (Table S4). We therefore find that while the input to the atmosphere from the deep mineral reservoir was 190 Mmol/a in 2008 (Figure 4), the removal in the deep ocean to the deep mineral reservoir was not substantially different from that of the preindustrial era (72 Mmol/a; Table S4). Given the overall residence time of Se in the ocean, it would take at least ~10^4 years for the ocean to come to steady state under a scenario of constant inputs.

With the model, we calculate a global average increase in total Se in the upper ocean (surface plus intermediate waters) of 3.2% due to anthropogenic emissions, which is smaller than estimated from the ocean profiles collected in 1977 and 2011 (10%–20%) for the subthermocline waters of the North Pacific Ocean (see section 3.3). Such differences likely reflect the differences in the global distribution of anthropogenic sources. As discussed in section 3.3, the Northern Hemisphere has been more influenced by anthropogenic Se releases than the Southern Hemisphere.

While the magnitude of the anthropogenic Se inputs has not yet had a dramatic impact on deep ocean Se concentrations, we can use the model to provide insights into the impact of various transport mechanisms. While the inorganic Se reservoirs in the deep ocean have increased by <0.1%, the particulate Se has increased by about 3%, a value similar to that of the upper ocean (Table S4). This difference reflects the *short-circuiting* of the particulate flux, which is essentially unidirectional, while the exchange between the ocean reservoirs for the other Se forms is bidirectional. Additionally, the burial of particulate Se into the ocean sediment has similarly increased more than the other transformation and deposition fluxes. This result illustrates the importance of particulate transport in changing Se concentrations in the deep ocean.

In conclusion, the model reflects the interpretation of existing data on the current impact of anthropogenic inputs of Se to the biosphere on the ocean Se inventory. Upper ocean Se concentrations have increased to some degree due to anthropogenic activities. The actual extent of change is likely a function of location and reflects recent industrialization in Asia and more emissions controls in North America and Europe. The increased concentrations of Se in the surface ocean have likely not enhanced productivity yet, but the possibility that this will happen in the future should be further investigated. Additionally, photochemical transformations appear to be important in the fate of methylated Se compounds such as $(CH_3)_2Se$, but they play little role in the speciation and transformations of inorganic Se. Our results suggest that Se (VI) uptake into phytoplankton is occurring in the ocean and this process should be further investigated. Additionally, given the relatively high concentrations of reduced Se in plankton, further studies should focus on the impact of reduced Se compounds on the cycling of metals that bind strongly with reduced S and Se.

Acknowledgments
The authors thank the captain, crew, and science party of the R/V *Kilo Moana* (*Metzyme* cruise), the USCGC *Healy* (Arctic cruise), and R/V *Connecticut* (LIS samples) for their help with water sampling during the cruises, and other laboratory members involved in coastal water sample collections, mainly in conjunction with the NIH/NIEHS funded Dartmouth Superfund Research Program (grant P42 ES007373). This study was partially funded by the National Science Foundation (NSF) Chemical Oceanography Program through grants 1130711 and 1434998 to R. P. M., and A. L. S. acknowledges financial support from the Swedish Research Council Formas (grant 2016-00875). The photochemical studies and field measurements were part of B.D.'s PhD thesis research. The model development began while R. P. M. was on sabbatical at Harvard University, and A. L. S. was a postdoc, with assistance from Elsie Sunderland and her research group. We thank Michelle Fogarty and Brandon Russell for assistance with HydroLight modeling, Bridget Holohan, Nashat Mazrui, and Kathleen Gosnell for assistance with nitrate and DOC analyses, and Whitney King for the use of his solar simulator. Data from this project have been submitted for archiving at the Biological and Chemical Oceanography Data Management office (BCO-DMO) in accordance with NSF policies and are available without restriction at https://www.bco-dmo.org/project/749366.

References

Allen, A. P., & Gillooly, J. F. (2006). Assessing latitudinal gradients in speciation rates and biodiversity at the global scale. *Ecology Letters*, *9*, 947–954. https://doi.org/10.1111/j.1461-0248.2006.00946.x

Amos, H. A., Sonke, J. E., Obrist, D., Robins, N., Hagan, N., Horowircz, H. M., et al. (2015). Observational and modeling constraints on global anthropogenic enrichment of mercury. *Environmental Science & Technology*, *49*(7), 4036–4047. https://doi.org/10.1021/es5058665

Amos, H. M., Jacob, D. J., Streets, D. G., & Sunderland, E. M. (2013). Legacy impacts of all-time anthropogenic emissions on the global mercury cycle. *Global Biogeochemical Cycles*, *27*, 410–421. https://doi.org/10.1002/gbc.20040

Amouroux, D., & Donard, O. F. X. (1996). Maritime emission of selenium to the atmosphere in eastern Mediterranean seas. *Geophysical Research Letters*, *23*(14), 1777–1780. https://doi.org/10.1029/96GL01271

Amouroux, D., & Donard, O. F. X. (1997). Evasion of selenium to the atmosphere via biomethylation processes in the Gironde estuary, France. *Marine Chemistry*, *58*, 173–188. https://doi.org/10.1016/S0304-4203(97)00033-9

Amouroux, D., Liss, P., Tessier, E., Hamren-Larsson, M., & Donard, O. F. X. (2001). Role of oceans as biogenic sources of selenium. *Earth and Planetary Science Letters*, *189*, 277–283. https://doi.org/10.1016/S0012-821X(01)00370-3

Amouroux, D., Pécheyran, C., & Donard, O. F. X. (2000). Formation of volatile selenium species in synthetic seawater under light and dark experimental conditions. *Applied Organometallic Chemistry*, *14*, 236–244.

Amouroux, D., Tessier, E., Pécheyran, C., & Donard, O. F. X. (1998). Sampling and probing volatile metal (loid) species in natural waters by in-situ purge and cryogenic trapping followed by gas chromatography and inductively coupled plasma mass spectrometry (P-CT–GC–ICP/MS). *Analytica Chimica Acta*, *377*, 241–254. https://doi.org/10.1016/S0003-2670(98)00425-5

Araie, H., & Shiraiwa, Y. (2009). Selenium utilization by microalgae. *Molecules*, *14*, 4880–4891.

Arimoto, R., Gao, Y., Zhou, M.-Y., Soo, D., Chen, L., Gu, D., et al. (1997). Atmospheric deposition of trace elements to the western Pacific basin. In J. E. Baker (Ed.), *Atmospheric deposition of contaminants to the great lakes and coastal waters*, (pp. 209–225). Pensacola: SETAC Press.

Baines, S. B., Fisher, N. S., Doblin, M. A., & Cutter, G. A. (2001). Uptake of dissolved organic selenides by marine phytoplankton. *Limnology and Oceanography*, *46*(8), 1936–1944.

Balzano, S., Statham, P. J., Pancost, R. D., & Lloyd, J. R. (2009). Role of microbial populations in the release of reduced iron to the water column from marine aggregates. *Aquatic Microbial Ecology*, *54*(3), 291–303.

Black, F. J., Poulin, B. A., & Flegal, A. R. (2012). Factors controlling the abiotic photo-degradation of monomethylmercury in surface waters. *Geochimica et Cosmochimica Acta*. https://doi.org/10.1016/j.gca.2012.01.019

Bouillon, R.-C., Miller, W. L., Levasseur, M., Scarratt, M., Merzouk, A., Michaud, S., & Ziolkowski, L. (2006). The effect of mesoscale iron enrichment on the marine photochemistry of dimethylsulfide in the NE subarctic Pacific. *Deep Sea Research Part II*, *53*, 2384–2397. https://doi.org/10.1016/j.dsr2.2006.05.024

Boyle, E., Lee, J.-M., Echegoyen, Y., Noble, A., Moos, S., Carrasco, G., et al. (2014). Anthropogenic lead emissions in the ocean: The evolving global experiment. *Oceanography*, *27*, 69–75.

Broecker, W. S., & Peng, T.-H. (1982). *Tracers in the Sea*. NY: Eldigio Press.

Carpenter, L. J., Archer, S. D., & Beale, R. (2012). Ocean-atmosphere trace gas exchange. *Chemical Society Reviews*, *41*(19), 6473–6506.

Chester, R., & Jickells, T. (2012). *Marine geochemistry*, (p. 411). Chichester, UK: Wiley-Blackwell.

Conde, J. E., & Alaejos, M. S. (1997). Selenium concentrations in natural and environmental waters. *Chemical Reviews*, *97*, 1979–2003.

Cutter, G. A. (1982). Selenium in reducing waters. *Science*, *217*, 829–831.

Cutter, G. A. (1992). Kinetic controls on the speciation of metalloids in seawater. *Marine Chemistry*, *40*, 65–80.

Cutter, G. A. (1993). Metalloids in wet deposition on Bermuda: Concentrations, sources, and fluxes. *Journal of Geophysical Research*, *98*, 16,777–16,710. https://doi.org/10.1029/93JD01689

Cutter, G. A. (2005). Biogeochemistry: Now and into the future. *Palaeogeography Palaeoclimatology Palaeoecology*, *219*, 191–198.

Cutter, G. A., & Bruland, K. W. (1984). The marine biogeochemistry of selenium: A re-evaluation. *Limnology and Oceanography*, *29*, 1179–1192.

Cutter, G. A., & Church, T. M. (1986). Selenium in western Atlantic precipitation. *Nature*, *322*, 720–722. https://doi.org/10.1038/322720a0

Cutter, G. A., & Cutter, L. S. (1995). Behavior of dissolved antimony, arsenic, and selenium in the Atlantic Ocean. *Marine Chemistry*, *49*, 295–306. https://doi.org/10.1016/0304-4203(95)00019-n

Cutter, G. A., & Cutter, L. S. (2001). Sources and cycling of selenium in the western and equatorial Atlantic Ocean. *Deep-Sea Research*, *48*, 2917–2931.

Danbara, A., & Shiraiwa, Y. (1999). The requirement of selenium for the growth of marine coccolithophorids, *Emiliania huxleyi*, *Gephyrocapsa oceanica* and *Helladosphaera* sp.(Prymnesiophyceae). *Plant and Cell Physiology*, *40*, 762–766.

DiMento, B., & Mason, R. P. (2017). Factors controlling the photochemical degradation of methylmercury in coastal and oceanic waters. *Marine Chemistry*, *196*, 116–125.

Doblin, M. A., Blackburn, S. I., & Hallegraeff, G. (1999). Comparative study of selenium requirements of three phytoplankton species: *Gymnodinium catenatum*, *Alexandrium minutum* (Dinophyta) and *Chaetoceros cf. tenuissimus* (Bacillariophyta). *Journal of Plankton Research*, *21*, 1153–1169. https://doi.org/10.1093/plankt/21.6.1153

Fernández-Gómez, C., Drott, A., Björn, E., Díez, S., Bayona, J. M., Tesfalidet, S., et al. (2013). Towards universal wavelength-specific photodegradation rate constants for methyl mercury in humic waters, exemplified by a boreal lake-wetland gradient. *Environmental Science & Technology*, *47*, 6279–6287. https://doi.org/10.1021/es400373s

Floor, G. H., & Roman-Ross, G. (2012). Selenium in volcanic environments: A review. *Applied Geochemistry*, *27*, 517–531.

Fournier, E., Adam-Guillermin, C., Potin-Gautier, M., & Pannier, F. (2010). Selenate bioaccumulation and toxicity in Chlamydomonas reinhardtii: Influence of ambient sulphate ion concentration. *Aquatic Toxicology*, *97*, 51–57.

Frouin, R., McPherson, J., Ueyoshi, K., & Franz, B. A. (2012). A time series of photosynthetically available radiation at the ocean surface from SeaWiFS and MODIS data. In R. J. Frouin, N. Ebuchi, D. Pan, & T. Saino (Eds.), *Presented at the SPIE Asia-Pacific remote sensing*, (852519–12). SPIE. https://doi.org/10.1117/12.981264

Gaillardet, J., Viers, J., & Dupré, B. (2003). Trace elements in river waters. In *Treatise on geochemistry*, (pp. 225–272). New York: Elsevier. https://doi.org/10.1016/B0-08-043751-6/05165-3

Gobler, C. J., Lobanov, A. V., Tang, Y.-Z., Turanov, A. A., Zhang, Y., Doblin, M., et al. (2013). The central role of selenium in the biochemistry and ecology of the harmful pelagophyte, *Aureococcus anophagefferens*. *The ISME Journal*, *7*, 1333–1343. https://doi.org/10.1038/ismej.2013.25

Gordeev, V. V., & Lisitzin, A. P. (2014). Geochemical interaction between the freshwater and marine hydrosphere. *Russian Geology and Geophysics*, *55*, 562–581.

Gosnell, K., & Mason, R. P. (2015). Mercury and methylmercury incidence and bioaccumulation in plankton from the central Pacific Ocean. *Marine Chemistry*, *177*, 772–780.

Guo, X., Sturgeon, R. E., Mester, Z., & Gardner, G. J. (2003a). Photochemical alkylation of inorganic selenium in the presence of low molecular weight organic acids. *Environmental Science & Technology*, *37*, 5645–5650.

Guo, X., Sturgeon, R. E., Mester, Z., & Gardner, G. J. (2003b). UV light-mediated alkylation of inorganic selenium. *Applied Organometallic Chemistry*, *17*, 575–579. https://doi.org/10.1002/aoc.473

Harrison, P. J., Yu, P. W., Thompson, P. A., Price, N. M., & Phillips, D. J. (1988). Survey of selenium requirements in marine phytoplankton. *Marine Ecology Progress Series*, *47*, 89–96.

Hatfield, D., & Gladyshev, V. (2002). How selenium has altered our understanding of the genetic code. *Molecular and Cellular Biology*, *22*, 3565–3576.

Hatfield, D. L., Lee, B. J., Price, N. M., & Stadtman, T. C. (1991). Selenocysteyl-tRNA occurs in the diatom *Thalassiosira* and in the ciliate *Tetrahymena*. *Molecular Microbiology*, *5*(5), 1183–1186.
Hu, M., Yang, Y., Martin, J. M., Yin, K., & Harrison, P. J. (1996). Preferential uptake of Se (IV) over Se (VI) and the production of dissolved organic Se by marine phytoplankton. *Marine Environmental Research*, *44*, 225–231. https://doi.org/10.1016/s0141-1136(97)00005-6
Kamp, A., Stief, P., Bristow, L. A., Thamdrup, B., & Glud, R. N. (2016). Intracellular nitrate of marine diatoms as a driver of anaerobic nitrogen cycling in sinking aggregates. *Frontiers in Microbiology*, *7*, 79–13. https://doi.org/10.3389/fmicb.2016.01669
Kester, D. R., Duedall, I. W., Connors, D. N., & Pytkowicz, R. M. (1967). Preparation of artificial seawater. *Limnology and Oceanography*, *12*, 176–179. https://doi.org/10.2307/2833179?ref=no-x-route:d3ac9fce08c02cda5c5e52589e8f8a2d
Khan, M. A. K., & Wang, F. (2009). Mercury-selenium compounds and their toxicological significance: Toward a molecular understanding of the mercury-selenium antagonism. *Environmental Toxicology and Chemistry*, *28*(8), 1567–1577.
Kieber, D. J., Jiao, J., Kiene, R. P., & Bates, T. S. (1996). Impact of dimethylsulfide photochemistry on methyl sulfur cycling in the equatorial Pacific Ocean. *Journal of Geophysical Research*, *101*, 3715–3722.
Lam, P. J., Lee, J.-M., Heller, M. I., Mehic, S., Xiang, Y., & Bates, N. R. (2018). Size-fractionated distributions of suspended particle concentration and major phase composition from the U.S. GEOTRACES Eastern Pacific Zonal Transect (GP16). *Marine Chemistry*, *201*, 90–107.
Laurier, F. J. G., Mason, R. P., Gill, G. A., & Whalin, L. (2004). Mercury distributions in the North Pacific Ocean—20 years of observations. *Marine Chemistry*, *90*(1–4), 3–19.
Luxem, K. E., Vriens, B., Behra, R., & Winkel, L. H. E. (2017). Studying selenium and sulfur volatilisation by marine algae *Emiliania huxleyi* and *Thalassiosira oceanica* in culture. *Environment and Chemistry*, *14*, 199–206.
Mason, R. P. (2013). *Trace metals in aquatic systems. John*, (p. 431). Chichester: Wiley-Blackwell.
Mason, R. P., Choi, A. L., Fitzgerald, W. F., Hammerschmidt, C. R., Lamborg, C. H., & Sunderland, E. M. (2012). Mercury biogeochemical cycling in the ocean and policy implications. *Environmental Research*, *119*, 03.013.
Measures, C. I., & Burton, J. D. (1980). The vertical distribution and oxidation states of dissolved selenium in the northeast Atlantic Ocean and their relationship to biological processes. *Earth and Planetary Science Letters*, *46*, 385–396. https://doi.org/10.1016/0012-821X(80)90052-7
Measures, C. I., Grant, B. C., Mangum, B. J., & Edmond, J. M. (1983). The Relationship of the distribution of dissolved selenium IV and VI in three oceans to physical and biological processes. In C. S. Wong, E. Boyle, K. W. Bruland, J. D. Burton, & E. D. Goldberg (Eds.), *Trace Metals in Sea Water. NATO Conference Series (IV Marine Sciences)*, (Vol. 9, pp. 78–83). Boston, MA: Springer.
Measures, C. I., McDuff, R. E., & Edmond, J. M. (1980). Selenium redox chemistry at GEOSECS I re-occupation. *Earth and Planetary Science Letters*, *49*, 102–108. https://doi.org/10.1016/0012-821X(80)90152-1
Mitrovic, S. M., Fernández Amandi, M., McKenzie, L., Furey, A., & James, K. J. (2004). Effects of selenium, iron and cobalt addition to growth and yessotoxin production of the toxic marine dinoflagellate *Protoceratium reticulatum* in culture. *Journal of Experimental Marine Biology and Ecology*, *313*, 337–351.
Morford, J. L., Martin, W. R., Francois, R., & Carney, C. M. (2009). A model for uranium, rhenium, and molybdenum diagenesis in marine sediments based on results from coastal locations. *Geochimica et Cosmochimica Acta*, *73*, 2938–2960.
Mosher, B. W., Duce, R. A., Prospero, J. M., & Savoie, D. L. (1987). Atmospheric selenium: Geographical distribution and ocean to atmosphere flux in the Pacific. *Journal of Geophysical Research*, *92*, 13,277–13,287.
Munson, K. M., Lamborg, C. H., Swarr, G. J., & Saito, M. A. (2015). Mercury species concentrations and fluxes in the central tropical Pacific Ocean. *Global Biogeochemical Cycles*, *29*, 656–676. https://doi.org/10.1002/2015GB005120
Nightingale, P. D., & Liss, P. S. (2004). Gases in seawater. In H. Elderfield (Ed.), *The oceans and marine geochemistry: Part of the treatise on geochemistry*, (pp. 49–81). Amsterdam: Elsevier.
Oremland, R. S., Blum, J. S., Bindi, A. B., Dowdle, P. R., Herbel, M., & Stolz, J. F. (1999). Simultaneous reduction of nitrate and selenate by cell suspensions of selenium-respiring bacteria. *Applied and Environmental Microbiology*, *65*, 4385–4392.
Pécheyran, C., Amouroux, D., & Donard, O. F. X. (1998). Field determination of volatile selenium species at ultra trace levels in environmental waters by on-line purging, cryofocusing and detection by atomic fluorescence spectroscopy. *Journal of Analytical Atomic Spectrometry*, *13*, 615–621. https://doi.org/10.1039/a802246a
Plant, J. A., Kinniburgh, D. G., Smedley, P. L., Fordyce, F. M., & Klinck, B. A. (2003). Arsenic and selenium. In *Treatise on geochemistry*, (pp. 17–66). New York: Elsevier. https://doi.org/10.1016/B0-08-043751-6/09047-2
Poste, A. E., Braaten, H. F. V., de Wit, H. A., Sørensen, K., & Larssen, T. (2015). Effects of photodemethylation on the methylmercury budget of boreal Norwegian lakes. *Environmental Toxicology and Chemistry*, *34*, 1213–1223. https://doi.org/10.1002/etc.2923
Price, N. M., Thompson, P. A., & Harrison, P. J. (1987). Selenium: An essential element for growth of the coastal marine diatom *Thalassiosira pseudonana* (Bacillariophyceae). *Journal of Phycology*, *23*, 1–9.
Ranville, M. A., Cutter, G. A., Buck, C. S., Landing, W. M., Cutter, L. S., Resing, J. A., & Flegal, A. R. (2010). Aeolian contamination of Se and Ag in the North Pacific from Asian fossil fuel combustion. *Environmental Science & Technology*, *44*, 1587–1593. https://doi.org/10.1021/es902523m
Scudlark, J. R., & Church, T. M. (1997). Atmospheric deposition of trace elements to the Mid-Atlantic Bight. In J. E. Baker (Ed.), *Atmospheric deposition of contaminants to the great lakes and coastal waters*, (pp. 195–208). Pensacola, florida, USA: SETAC Press.
Sherrard, J. C., Hunter, K. A., & Boyd, P. W. (2004). Selenium speciation in sub-Antarctic and subtropical waters east of New Zealand: Trends and temporal variations. *Deep Sea Research Part I: Oceanographic Research Papers*, *51*, 491–506. https://doi.org/10.1016/j.dsr.2003.11.001
Soerensen, A., Sunderland, E. M., Holmes, C. D., Jacob, D. J., Yantosca, R. M., Skov, H., et al. (2010). An improved global model for air-sea exchange of mercury: High concentrations over the North Atlantic. *Environmental Science & Technology*, *44*(22), 8574–8580. https://doi.org/10.1021/es102032g
Soerensen, A. L., Mason, R. P., Balcom, P. H., Jacob, D. J., Zhang, Y., Kuss, J., & Sunderland, E. M. (2014). Elemental mercury concentrations and fluxes in the tropical atmosphere and ocean. *Environmental Science & Technology*, *48*, 11,312–11,319. https://doi.org/10.1021/es503109p
Sonnerup, R. E., Bullister, J. L., & Warmer, M. J. (2008). Improved estimates of ventilation rate changes and CO_2 uptake in the Pacific Ocean using chlorofluorocarbons and sulfur hexafluoride. *Journal of Geophysical Research*, *113*, C12007. https://doi.org/10.1029/2008JC004864
Sonnerup, R. E., Mecking, S., & Bullister, J. L. (2013). Transit time distributions and oxygen utilization rates in the Northeast Pacific Ocean from chlorofluorocarbons and sulfur hexafluoride. *Deep-Sea Research Part I: Oceanographic Research Papers*, *72*, 61–71.
Sonnerup, R. E., Mecking, S., Bullister, J. L., & Warner, M. J. (2015). Transit time distributions and oxygen utilization rates from chlorofluorocarbons and sulfur hexafluoride in the Southeast Pacific Ocean. *Journal of Geophysical Research: Oceans*, *120*, 3761–3776. https://doi.org/10.1002/2015JC010781
Stefels, J., Steinke, M., Turner, S., Malin, G., & Belviso, S. (2007). Environmental constraints on the production and removal of the climatically active gas dimethylsulphide (DMS) and implications for ecosystem modelling. *Biogeochemistry*, *83*(1–3), 245–275.
Stolz, J. (2016). Geomicrobiology of selenium and tellurium. In H. L. Ehrlich, D. K. Newman, & A. Kapple (Eds.), *Ehrlich's Geomicrobiology*, (6th ed.pp. 551–564). Boca Raton: CRC Press.

Stolz, J. E., Basu, P., Santini, J. M., & Oremland, R. S. (2006). Arsenic and selenium in microbial metabolism. *Annual Review of Microbiology*, *60*, 107–130.

Stueken, E. E. (2017). Selenium isotopes as a biogeochemcial proxy in deep time. *Reviews in Mineralogy and Geochemistry*, *82*, 657–682.

Stueken, E. E., Buick, R., Bekker, A., Catling, D., Foriel, J., Guy, B. M., et al. (2015). The evolution of the global selenium cycle: Secular trends in Se isotopes and abundances. *Geochimica et Cosmochimica Acta*, *62*, 109–125.

Sunderland, E. M., Dalziel, J., Heyes, A., Branfireun, B. A., Krabbenhoft, D. P., & Gobas, F. A. (2010). Response of a Macrotidal Estuary to Changes in Anthropogenic MercuryLoading between 1850 and 2000. *Environmental Science and Technology*, *44*(5), 1698–704. https://doi.org/10.1021/es9032524

Sunderland, E. M., Krabbenhoft, D. P., Moreau, J. W., Strode, S. A., & Landing, W. M. (2009). Mercury sources, distribution, and bioavailability in the North Pacific Ocean: Insights from data and models. *Global Biogeochemical Cycles*, *23*, GB2010. https://doi.org/10.1029/2008GB003425

Taalba, A., Xie, H., Scarratt, M. G., Bélanger, S., & Levasseur, M. (2013). Photooxidation of dimethylsulfide (DMS) in the Canadian Arctic. *Biogeosciences Discussions*, *10*, 2093–2126. https://doi.org/10.5194/bgd-10-2093-2013

Tanzer, D., & Heumann, K. G. (1991). Determination of dissolved selenium species in environmental water samples using isotope dilution mass spectrometry. *Analytical Chemistry*, *63*, 1984–1989.

Tessier, E., Amouroux, D., & Donard, O. F. X. (2002). Biogenic volatilization of trace elements from European estuaries. *ACS Symposium Series*, *835*, 151–165.

Toole, D. A., Kieber, D. J., Kiene, R. P., White, E. M., Bisgrove, J., del Valle, D. A., & Slezak, D. (2004). High dimethylsulfide photolysis rates in nitrate-rich Antarctic waters. *Geophysical Research Letters*, *31*, L11307. https://doi.org/10.1029/2004GL019863

Toole, D. A., Kieber, D. J., Kiene, R. P., Siegel, D. A., & Nelson, N. B. (2003). Photolysis and the dimethylsulfide (DMS) summer paradox in the Sargasso Sea. *Limnology and Oceanography*, *48*, 1088–1100. https://doi.org/10.4319/lo.2003.48.3.1088

Toole, D. A., Slezak, D., Kiene, R. P., Kieber, D. J., & Siegel, D. A. (2006). Effects of solar radiation on dimethylsulfide cycling in the western Atlantic Ocean. *Deep Sea Research Part I: Oceanographic Research Papers*, *53*, 136–153. https://doi.org/10.1016/j.dsr.2005.09.003

Velinsky, D. J., & Cutter, G. A. (1991). Geochemistry of selenium in a coastal salt marsh. *Geochimica et Cosmochimica Acta*, *55*, 179–191.

Vriens, B., Lenz, M., Charlet, L., Berg, M., & Winkel, L. H. E. (2014). Natural wetland emissions of methylated trace elements. *Nature Communications*, *5*.

Wake, B. D., Hassler, C. S., & Bowie, A. R. (2012). Phytoplankton selenium requirements: The case for species isolated from temperate and polar regions of the Southern Ocean. *Journal of Phycology*. https://doi.org/10.1111/j.1529-8817.2012.01153.x

Wen, H., & Carignan, J. (2007). Reviews on atmospheric selenium: Emissions, speciation and fate. *Atmospheric Environment*, *41*, 7151–7165. https://doi.org/10.1016/j.atmosenv.2007.07.035

Wheeler, A. E., Zingaro, R. A., Irgolic, K., & Bottino, N. R. (1982). The effect of selenate, selenite, and sulfate on the growth of six unicellular marine algae. *Journal of Experimental Marine Biology and Ecology*, *57*, 181–194. https://doi.org/10.1016/0022-0981(82)90191-5

Winkel, L. H. E., Vriens, B., Jones, G., Schneider, L., Pilon-Smits, E., & Bañuelos, G. (2015). Selenium cycling across soil-plant-atmosphere interfaces: A critical review. *Nutrients*, *7*(6), 4199–4239. https://doi.org/10.3390/nu7064199

Zepp, R. G., Hoigné, J., & Bader, H. (1987). Nitrate-induced photooxidation of trace organic chemicals in water. *Environmental Science & Technology*, *21*, 443–450. https://doi.org/10.1021/es00159a004

Zepp, R. G., Faust, B. C., & Hoigne, J. (1992). Hydroxyl radical formation in aqueous reactions (pH 3-8) of iron (II) with hydrogen peroxide: The photo-Fenton reaction. *Environmental Science & Technology*, *26*, 313–319. https://doi.org/10.1021/es00026a011

Zhang, Y., & Gladyshev, V. N. (2008). Trends in selenium utilization in marine microbial world revealed through the analysis of the global ocean sampling (GOS) project. *PLoS Genetics*, *4*, e1000095. https://doi.org/10.1371/journal.pgen.1000095

Zhao, Q.-X., Chen, Y.-W., Belzile, N., & Wang, M. (2010). Low volume microwave digestion and direct determination of selenium in biological samples by hydride generation-atomic fluorescence spectrometry. *Analytica Chimica Acta*, *665*, 123–128. https://doi.org/10.1016/j.aca.2010.03.040

Zurbick, C. M., Gallon, C., & Flegal, A. R. (2017). Historic and industrial lead within the Northwest Pacific Ocean evidenced by lead isotopes in seawater. *Environmental Science & Technology*, *51*, 1203–1212.